New archaeomagnetic data recovered from the study of Roman and Visigothic remains from central Spain (3rd-7th centuries)

Gianluca Catanzariti, Miriam Gomez-Paccard, Greg Mcintosh, Francisco J. Pavon-Carrasco, Annick Chauvin, Maria. L. Osete

Geophysical Journal International

Geophys. J. Int. (2012) **188,** 979–993 doi: 10.1111/j.1365-246X.2011.05315.x

New archaeomagnetic data recovered from the study of Roman and Visigothic remains from central Spain (3rd–7th centuries)

Gianluca Catanzariti,[1] Miriam Gómez-Paccard,[2] Gregg McIntosh,[3,4] Francisco J. Pavón-Carrasco,[3,4] Annick Chauvin[5] and María L. Osete[3,4]

[1] *Centro de Arqueometría y Análisis Arqueológico, Facultad de Geografía e Historia, Universidad Complutense de Madrid, Profesor Aranguren s/n,* 28040 *Madrid, Spain. E-mail: gcatanza@fis.ucm.es*
[2] *Institut de Ciències de la Terra Jaume Almera, ICTJA-CSIC, Lluís Solé i Sabarís s/n,* 08028 *Barcelona, Spain*
[3] *Departamento de Física de la Tierra, Astronomía y Astrofísica I (Geofísica y Meteorología), Facultad de Ciencias Físicas, Universidad Complutense de Madrid, Avda Complutense s/n,* 28040 *Madrid, Spain*
[4] *Instituto de Geociencias (UCM-CSIC), Facultad de Ciencias Físicas, Universidad Complutense de Madrid, Avda Complutense s/n,* 28040 *Madrid, Spain*
[5] *Géosciences-Rennes, CNRS, UMR* 6118*, Université de Rennes* 1*, Campus de Beaulieu,* 35042 *Rennes, Cedex, France*

Accepted 2011 November 23. Received 2011 October 28; in original form 2011 August 3

SUMMARY

New archaeomagnetic results from four heated/combustion structures recovered from two archaeological sites in central Spain are reported. They have been dated by archaeological evidence and in two cases by radiocarbon dating. Rock magnetic experiments indicate low coercivity magnetic phases, such as magnetite and thermally stable maghaemite, as the main carriers of the remanent magnetization. Haematite has been observed in poorly heated baked clays. Archaeomagnetic directions have been obtained from either alternating field or thermal demagnetization experiments performed on 57 specimens coming from 46 independently oriented samples. The four well-defined archaeomagnetic directions obtained are in good agreement with previous archaeomagnetic data and with recent regional and global field models. They define the beginning of easterly declination drift that was initiated around 350–400 AD and culminated around 800–850 AD, and delineate the maximum in inclination that took place around 600–650 AD. In addition, classical Thellier–Thellier experiments including thermal remanent magnetization anisotropy and cooling rate corrections were conducted on 23 specimens. Only 13 specimens, corresponding to well-defined single component behaviour, gave reliable results. New mean archaeointensities have been obtained for two of the four studied structures (VBK1, 64.2 ± 5.0 μT and VBT1, 62.4 ± 2.6 μT). The new data suggest that two relative intensity maxima occurred in Western Europe around 320 and 630 AD, being of lower magnitude that observed in Eastern Europe.

Key words: Archaeomagnetism; Palaeomagnetic secular variation; Rock and mineral magnetism; Europe.

1 INTRODUCTION

Knowledge of the secular variation of the geomagnetic field in the Iberian Peninsula has been considerably improved over recent years and new archaeomagnetic directions and archaeointensities are now available for this region (Gómez-Paccard *et al*. 2006a,c, 2008; Catanzariti *et al*. 2007, 2008; Ruiz-Martinez *et al*. 2008; Hartmann *et al*. 2009). The archaeomagnetic directional database published by Gómez-Paccard *et al.* (2006a) has been used to propose the first archaeomagnetic secular variation curve for the Iberian Peninsula (Gómez-Paccard *et al*. 2006b). This curve was computed by Bayesian modelling using a total of 134 archaeomagnetic directions, with ages ranging from 775 to 1959 AD, coming from the Iberian Peninsula, Northern Morocco and Southern France. The recent archaeointensity data obtained for Spain (Gómez-Paccard *et al*. 2008) and Portugal (Hartmann *et al*. 2009) constitute the first systematic studies of archaeomagnetic material for this region that help to constrain the geomagnetic dipole moment evolution in Western Europe during the past 2000 yr.

Despite this effort, the Iberian archaeomagnetic data are still sparse in comparison with other countries where archaeomagnetism has a traditional history, such as France (Thellier & Thellier 1959; Bucur 1994; Gallet *et al*. 2002) or Bulgaria (Kovacheva *et al*. 1998; Kovacheva *et al*. 2009). This is especially relevant for the period spanning the 4th and the 10th centuries AD—and more significantly for archaeointensity data—for which a detailed evolution of geomagnetic field changes is still lacking. The scarcity of data for this time period is a problem not only in the Iberian Peninsula but also in Western Europe (Gómez-Paccard *et al*. 2006c, 2008; Genevey *et al*. 2008; Donadini *et al*. 2009).

Spain has a rich historical past and several archaeological sites corresponding to this period have been the subject of intensive archaeological investigation during the last years (e.g. Vigil-Escalera 2007; Ramírez-González 2008). This study has benefited from these investigations and focuses on the archaeomagnetic study of four heated/combustion structures recovered from two archaeological sites located in central Spain: Vega Baja (Toledo) and Ruiseñor (Guadalajara). The sites date back to the 3rd and the 7th centuries AD. The new archaeomagnetic directions and archaeointensities will enhance the Iberian and Western Europe datasets and will contribute to future refinement of the Iberian regional palaeosecular (PSV) curves and geomagnetic field models. In addition, better established PSV curves or geomagnetic field models will increase the precision of the archaeomagnetism-based dating method for this region (Pavón-Carrasco *et al*. 2011).

2 ARCHAEOLOGICAL CONTEXT AND DATING

2.1 Vega Baja

The archaeological site named Vega Baja (Toledo, Lat. 39.9° N, Long. 4.0° W) was revealed during the construction of a new urban project. The remains correspond to the suburbs of the ancient capital of the Hispano-Visigoth kingdom (507–725 AD). Parts of the Palatine complex (the San Pedro y San Pablo basilica), the Roman Circus and the old Santa Leocadia basilica were discovered, with chronologies between the 4th and 9th centuries AD (Rojas & Gómez-Laguna 2009).

The archaeological structures studied from this site consist of the remains of a hypocaust associated with a thermal bath complex (structure VBT1) and the combustion chamber of a kiln used to make ceramics (structure VBK1). The former (VBT1) is a burnt soil surface about 4 m long and 1.5 m wide representing part of the hypocaust floor. Zones with variable colouring can be distinguished. Dark brown colours are related to poorly consolidated baked sediments that include carbon fragments and ashes, and pale grey colours that are associated with highly calcinated, hard clay materials (Fig. 1a). The structure also includes remains from two *pilae* that supported the *caldarium* floor, part of the *preaefurnium* and some water draining structures.

The second structure studied (VBK1) consists of a pit of about 1.5 m long, 1 m wide and 1 m depth, surrounded by three walls covered by a baked clay surface that is 3–4 cm thick (Fig. 1b). A large amount of ceramic materials was recovered from the structure, indicating that it represents the *praefurnium* of a ceramic kiln. The firing chamber or other building elements have not been preserved. Both the hypocaust and the combustion chamber are *in situ* structures that were built using the same argillaceous sediments that compose the subsoil of the Vega Baja site. Depending on the firing temperatures these sediments have been transformed into baked clay material of variable hardness.

The VBT1 hypocaust structure has been dated on the basis of archaeological and stratigraphical evidence and by means of two radiometric analyses (^{14}C), which were carried out on different charcoal fragments taken from the baked hypocaust surface (Table 1). A *Terminus Ante Quem* was provided by several wall structures that cut the hypocaust surface at an upper stratigraphic level. Rojas & Gómez-Laguna (2009) relate these new structures to the second occupation phase of the site ('hispano-visigodo clásico'), falling between the second half of the 6th century and the first half of the 7th centuries AD.

The two ^{14}C ages provide a combined mean age that has been used to calculate the calendar age using the calibration software OxCal v 4.10 (Bronk Ramsey 2009) and the IntCal09 calibration curve (Reimer et al. 2009). This gives a calendar age of between 596 and 657 AD at the 95 per cent probability level.

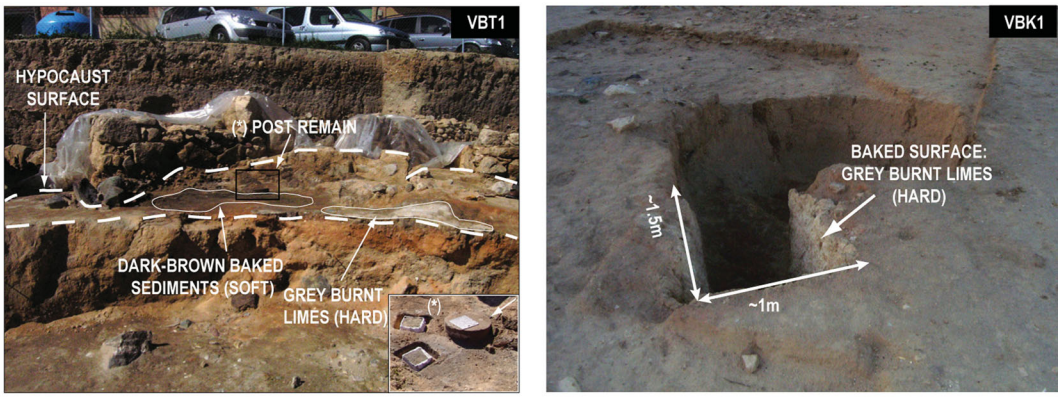

(a) (b)

Figure 1. Photographs of the structures sampled at Vega Baja. (a) VBT1 and (b) VBK1.

Table 1. Radiocarbon ages available from the Vega Baja archaeological site. CCR: Centre for Chronological Research, Nagoya University, Japan. CEDAD: Centro di Datazione e Diagnostica dell'Universitá del Salento, Lecce, Italy.

	Sample	Uncalibrated date	Combined calibrated date (at 95.4 per cent confidence level)	Laboratory
Hypocaust VBT1	UE323/INV167	1449 ± 27 BP	546–657 AD	CCR
	UE323 (LTL3438A)	1382 ± 35 BP		CEDAD
Kiln VBK1	UE23-UE1/INV1690BIS	1729 ± 27 BP	249–384 AD	CCR
	UE40.23 (LTL3439A)	1726 ± 35 BP		CEDAD

A combined calendar age of 249–384 AD (95 per cent probability level) has been determined from two charcoal fragments from kiln VBK1, following the same procedure. This has been taken as the age of the last use of the kiln (Table 1).

2.2 Ruiseñor

The Ruiseñor archaeological site (Guadalajara, Lat. 40.6° N, Long. 3.2° W) was revealed during construction of the new campus of Guadalajara University. It includes a Visigoth cemetery and the remains of a hamlet with grain silos and various burnt soils that may be associated with hearths/cooking ovens. The structures studied from this site are two combustion chambers, RSC1 and RSC4, directly excavated from the ground and interpreted as the remains of ovens used for cooking food (Ramírez-González 2008; Figs 2a and b). Both combustion chambers have a diameter of about 1 m. For RSC1, the bottom surface is located at a depth of 40–50 cm below this ground surface, whilst for RSC4 the bottom surface is located at a depth of about 30 cm. The bottom surface of RSC1 is covered with a layer of tile fragments, whereas an ash horizon is present on the bottom surface of RSC4. The materials are represented by poorly consolidate baked clay sediments containing a sandy fraction.

The chronology of the studied ovens (RSC1 and RSC4) is based on archaeological criteria, ceramics associated with the ovens, and on analogies with other archaeological sites from central Iberia, such as the 'Vega' of Jarama, Guadarrama and Henares (Vigil-Escalera 2007). The layout of the site is considered typical of small Visigoth villages that existed in Iberia from the end of the 5th century AD up to the 7th century AD (Ramirez-González 2008). The ovens are associated with negative structures related to cabin basements excavated into the ground, small silos for grain storage and water wells. Such features are considered the classic configuration of Visigoth villages. At Ruiseñor, this chronology is corroborated by a Visigothic cemetery including several tombs, all aligned in a W–E direction, where typical Visigothic jewels have been found. Therefore the last use of both structures has been placed within a large interval: 450–700 AD. The archaeological information is not sufficient to establish a more precise chronology for the abandonment of the structures.

3 SAMPLING AND LABORATORY PROTOCOLS

3.1 Sampling

Samples taken from both sites consist of pseudo-rectangular blocks of baked argillaceous sediments of variable hardness, with size varying from several centimetres to a few decimetres. Samples from Ruiseñor (RSC1 and RSC4) include 21 independently oriented blocks of soft baked sediments and 10 oriented ceramic tile fragments (previously baked at high temperature and re-used as floor elements in the RSC1 combustion chamber). In contrast to the poorly consolidated baked sediments, tile fragments are referred to as hard materials. Samples from Vega Baja (VBT1 and VBK1) are 21 well-consolidated block samples with grey-red/pale colouration due to the intensive heating of the original argillaceous lithology, together with six soft samples whose material is a mixture of soft burnt argillaceous sediments with carbon fragments and ashes. Only hard samples were taken from the kiln VBK1.

Sampling of soft material taken from both sites has been carried out by means of gypsum bandages and plaster of Paris. In Figs 3(a) and (b) images describing the fieldwork at Vega Baja and Ruiseñor site are shown. Pseudo-rectangular blocks were first isolated from the surrounding ground, then vertical walls of each block were wrapped in gypsum bandages to give them a higher physical resistance. The upper faces were covered by a flat plaster surface (Fig. 3a). After drying, the upper surfaces were oriented using a magnetic compass and the lower surfaces were cut by means of a thin aluminium sheet. Similar procedures were followed for VBT1, RSC1 and RSC4, where the only difference resides in the sample position inside the structures (from the floor in the case of VBT1, from both the floor and wall for RSC1 and RSC4; Fig. 3b). The compass readings have been corrected by the local declination of the studied sites.

Sampling procedures were simpler for hard materials from RSC1 and VBK1. Here, flat plaster surfaces adhering on selected sampling points were prepared and oriented by a magnetic compass. Tile fragments from RSC1 were then manually taken off the structure whilst sample blocks from VBT1 were cut using an handsaw and a chisel.

Standard cubic palaeomagnetic specimens were cut at the University Complutense of Madrid obtaining at least one

(a) (b)

Figure 2. Photographs of the structures sampled at Ruiseñor. (a) RSC4 and (b) RSC1.

(a) (b)

Figure 3. Photograph showing the sampling protocol.

specimen from each sample. Soft materials were previously consolidated by impregnation in ethyl-slicate (commercial name Silbond 40).

3.2 Magnetic measurements

The archaeomagnetic directions and rock magnetic properties were studied in the Palaeomagnetism Laboratory of the Complutense University of Madrid (UCM). Archaeointensity determinations were carried out at the Palaeomagnetism Laboratories of the Institute of Earth Sciences Jaume Almera (UB-CSIC) in Barcelona, and Géosciences-Rennes (CNRS-Université de Rennes 1) in Rennes.

An AGICO JR5 spinner magnetometer and a 2G Enterprises 755–4K SRM cryogenic magnetometer were used to measure the natural remanent magnetization (NRM) of Ruiseñor and Vega Baja samples, respectively. Low field magnetic susceptibility (κ) of each specimen was measured using an AGICO KLY3 susceptibility meter. Stepwise thermal (TH) demagnetization of NRM was carried out using a Schonsted Instruments TSD-1 thermal demagnetizer in 30–60°C steps up to 580–680°C. Stepwise alternating field (AF) demagnetization was conducted using a Schonsted Instruments GSD-5 tumbling demagnetizer, in 5–20 mT steps up to the maximum available peak AF of 100 mT.

Additional rock-magnetic measurements were made using a Coercivity Meter (Iasonov *et al*. 1998), which generates magnetic hysteresis curves, along with stepwise acquisition and reverse-field acquisition of isothermal remanence (IRM) that allowed deriving the following parameters: coercivity (H_c), saturation magnetization (M_s), saturation remanence (M_{rs}) and coercivity of remanence (H_{cr}). The maximum applied field was 500 mT. A Petersen Instruments MMVFTB variable field translation balance was used to measure thermomagnetic curves. Magnetization was measured in an applied field of 107 mT, with heating and cooling carried out in air.

Parallel to the directional and rock magnetic studies, archaeointensity experiments involving all the different material typologies were carried out following the classical Thellier palaeointensity method (Thellier & Thellier 1959). This method is based on the comparison of the NRM lost and the partial thermoremanent magnetization (pTRM) gained in a known laboratory field at progressive higher temperature steps. Remanent magnetization was measured using a 2G Enterprises 755R SRM superconducting magnetometer. Specimens were heated in a Magnetic Measurements MMTD-80 thermal demagnetizer from 100°C to temperature up to 565°C. A laboratory field of 50 or 60 μT was applied along the Z axis of the specimens. Between 8 and 19 temperature steps were performed. TRM anisotropy tensor was calculated for each specimen from the acquisition of a TRM in six different directions. In order to avoid magneto-chemical changes the TRM anisotropy tensor was measured during the Thellier experiments at temperatures at which around 70 per cent of the NRM intensity is lost. The cooling rate dependence of TRM intensity was also determined by measuring four additional TRM acquisition steps after the end of Thellier experiments. Comparison between rapid (typical laboratory cooling time of about 1.5 hr) and slow cooling results (about 24 hr) allowed the quantification of the cooling rate effect upon archaeointensity estimates for each specimen. For a detailed description of the experimental procedures followed in the archaeointensity protocol see Gómez-Paccard *et al*. (2006c).

4 ROCK MAGNETIC RESULTS

Initial NRM intensity and κ vary between 3.5×10^{-3} and 8.0 A m^{-1} and between 5.1×10^{-5} and 0.12 SI. As shown in Fig. 4, where NRM versus κ is plotted together with constant lines of Koenigsberger ratios (Q_n), the parameters define a bimodal distribution that is related to the hardness of the sampled material. High NRM and κ values, typical for well-baked argillaceous materials, are observed for hard baked clays that include tile fragments from kiln RSC1, grey/red pale specimens from the hypocaust VBT1 and all the specimens from kiln VBK1. Lower values correspond to soft, baked clays from ovens RSC1 and RSC4, and to soft, dark brown specimens from the hypocaust VBT1. Values of Q_n between 1 and 100 support a thermoremanent origin of the NRM.

Representative samples of hard and soft material have been studied in more detail. Both types of samples exhibit hysteresis curves that reach reversible behaviour by 300 mT, beyond which the increase in magnetization has been considered as being dominated by paramagnetic behaviour and/or by high coercivity magnetic phases (Figs 5a and b). The parameters M_s and H_c have been calculated after high field correction, determined from the slope of the curve between 300 and 500 mT.

Hard baked clay and tile samples exhibit much higher concentration-dependent parameters than do soft material samples (Table 2). They exhibit IRM acquisition curves that approach saturation by 300 mT (Figs 5a and b). Values of H_c and H_{cr} range between 8–16 and 17–36 mT, respectively. Thermomagnetic curves exhibit a single slope change in both the heating and cooling curves

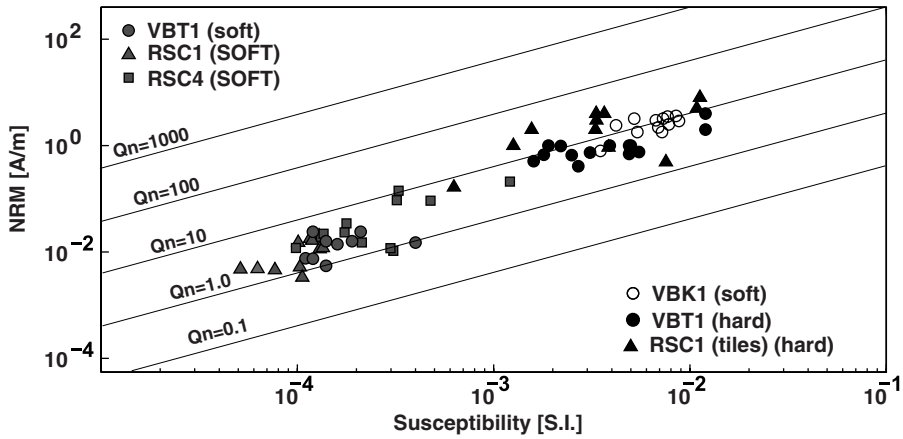

Figure 4. Intensity of natural remanent magnetization (NRM) versus bulk susceptibility (κ). Lines indicate constant Koenigsberger ratios between 0.1 and 1000.

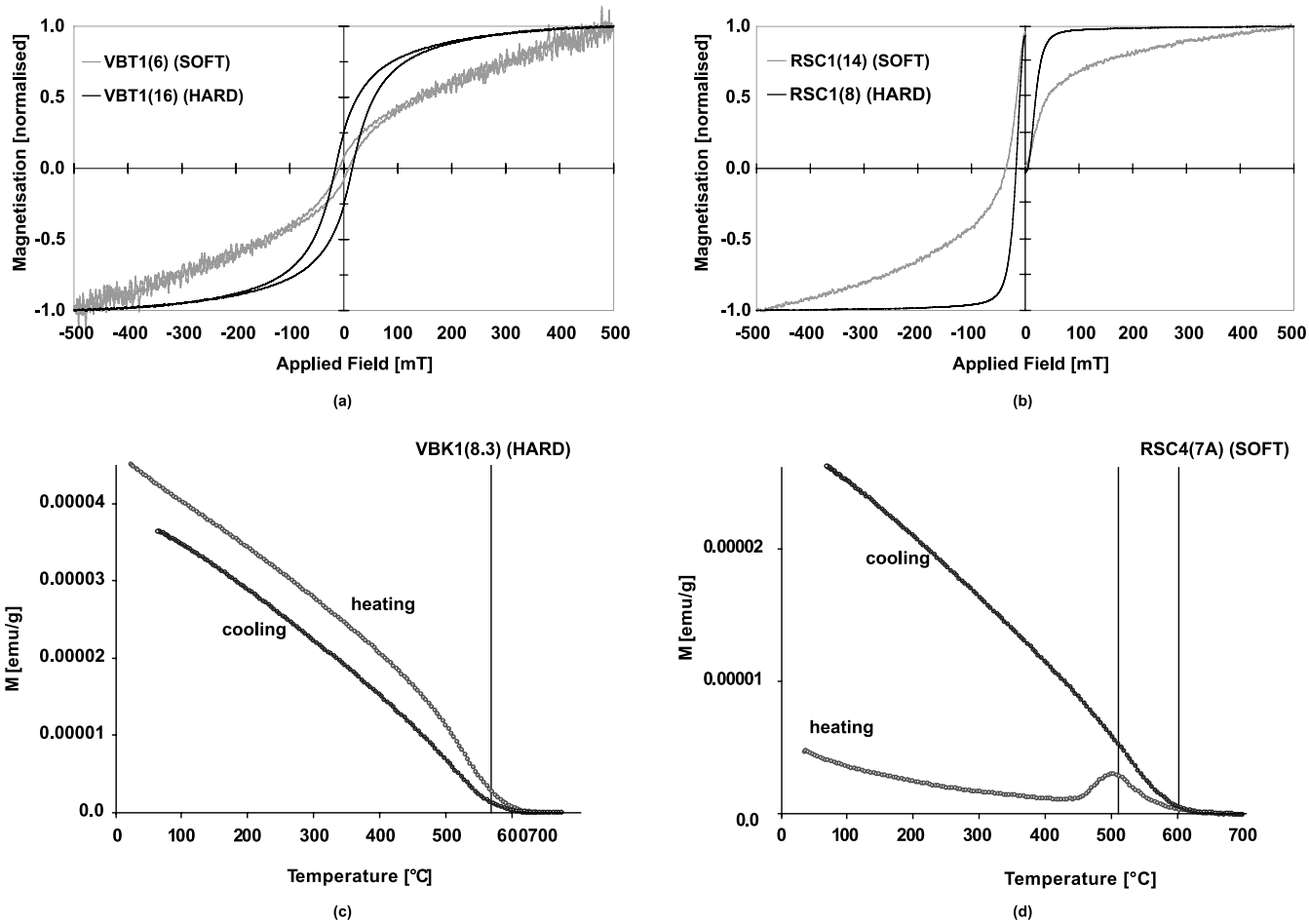

Figure 5. Representative rock magnetic results. (a) and (b) hysteresis curves, (c) and (d) normalized magnetization versus temperature curves.

(Fig. 5c). Curie temperatures, estimated from the heating curves using the second derivative of the heating curve (Tauxe 1998) of 578 and 630°C are observed. The thermomagnetic curves are approximately reversible, showing a minor loss in magnetization on cooling. Together with the low coercivities, this suggests that magnetite and thermally stable maghaemite are the magnetic carriers in the hard baked clays and tiles.

Soft baked clay samples are much less magnetic than the hard samples (Table 2). IRM acquisition curves do not reach saturation by 500 mT (Fig. 5b) and values for the S ratio ($S = -\mathrm{IRM}_{-0.3\mathrm{T}}/\mathrm{IRM}_{0.5\mathrm{T}}$) range between 0.77 and 0.93 (Table 2). They have H_c values of 8–12 mT and H_{cr} values of 25–36 mT. Thermomagnetic curves are highly non-reversible, showing a peak in magnetization on heating to 500 °C and an increase in magnetization on cooling. Curie

Table 2. Summary of rock magnetic properties of representative samples of hard and soft materials. The saturation magnetization (M_s), saturation remanence (M_{rs}), coercivity (H_c), coercivity of remanence (H_{cr}), S-ratio (defined as $-IRM_{-0.3T}/IRM_{0.5T}$) and Curie temperature (T_c) are given.

Sample	M_s (Am^2 kg^{-1})	M_{rs} (Am^2 kg^{-1})	H_c (mT)	H_{cr} (mT)	S ratio	T_c (°C)
VBK1-6 (hard)	0.186	3.26×10^{-2}	8.4	17.9	0.99	
VBK1-8 (hard)	0.204	5.29×10^{-2}	12.8	25.6	0.99	578
VBT1-14-2 (hard)	0.096	2.52×10^{-2}	15.9	33.0	0.99	
VBT1-16 (hard)	0.157	4.27×10^{-2}	15.8	36.3	0.99	630
RSC1-8C (hard)	0.252	6.44×10^{-2}	9.0	17.0	0.99	
VBT1-7-3 (soft)	5.06×10^{-3}	9.09×10^{-4}	10.4	26.8	0.93	
RSC1-14A (soft)	2.56×10^{-3}	3.84×10^{-4}	9.6	35.4	0.77	580
RSC1-16A (soft)	2.49×10^{-3}	4.51×10^{-4}	12.1	36.1	0.78	
RSC4-7A (soft)	4.36×10^{-3}	5.64×10^{-4}	8.2	30.2	0.83	578
RSC4-10B (soft)	4.05×10^{-3}	7.39×10^{-4}	9.3	24.8	0.87	

temperatures of 580–587 °C were calculated from the cooling curve (Fig. 5d). This suggests that magnetite was produced during heating, probably masking any contribution of the original magnetic minerals present in the samples. Rock magnetic tests do not identify the high coercivity phase(s). However, maximum unblocking temperatures of NRM of 650–680 °C for soft baked clay specimens (Section 5) strongly suggest haematite as the carrier of the high coercivity remanence.

5 ARCHAEOMAGNETIC DIRECTIONS

Well-grouped, northerly and positive initial NRM directions were obtained from the baked clay materials from all four structures (Figs 6a–c and e). In contrast, the tile specimens from RSC1 showed dispersed NRM directions (Fig. 6d).

At least one specimen per sample has been demagnetized. Representative plots of stepwise TH and AF demagnetization of the NRM and typical intensity decay curves are shown in Figs 7 and 8, respectively.

The behaviour during TH demagnetization varied in function of the type of sampled material. Hard baked clay specimens exhibited a single, stable component up to 580–630 °C comprising more than 95 per cent of the initial NRM (e.g. Figs 7a and b and 8a). Soft baked clay specimens had a well-defined, stable component up to 400–430 °C. For specimens from VBT1 this component represented more than 90 per cent of the initial NRM, with the remainder demagnetized by 580 °C (e.g., Figs 7c and 8a). For specimens from RSC1 and RSC4 this component carried 80–85 per cent of the initial NRM, along with an unstable component with maximum demagnetization temperatures of 650–680 °C (Figs 7h and l and 8c). The tile specimens from RSC1 exhibited two stable components between room temperature and 230–350 °C and between 300–350 and 580 °C (e.g. Figs 7i and j). Varying degrees of overlap between these two components were observed leading to curved demagnetization vectors in all but two specimens.

AF demagnetization of baked samples yielded better-defined demagnetization curves than TH demagnetization (e.g. Figs 7b, d, f, g and k). A stable component could be identified between 5

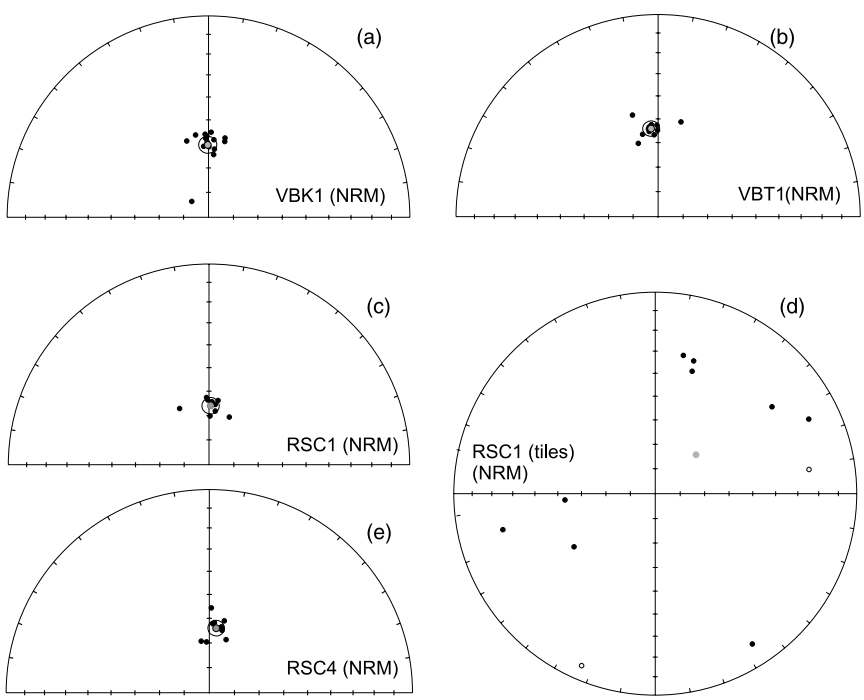

Figure 6. Initial natural remanent magnetization (NRM) directions measured for (a) VBK1, (b) VBT1, (c, d) RSC1 and (e) RSC4.

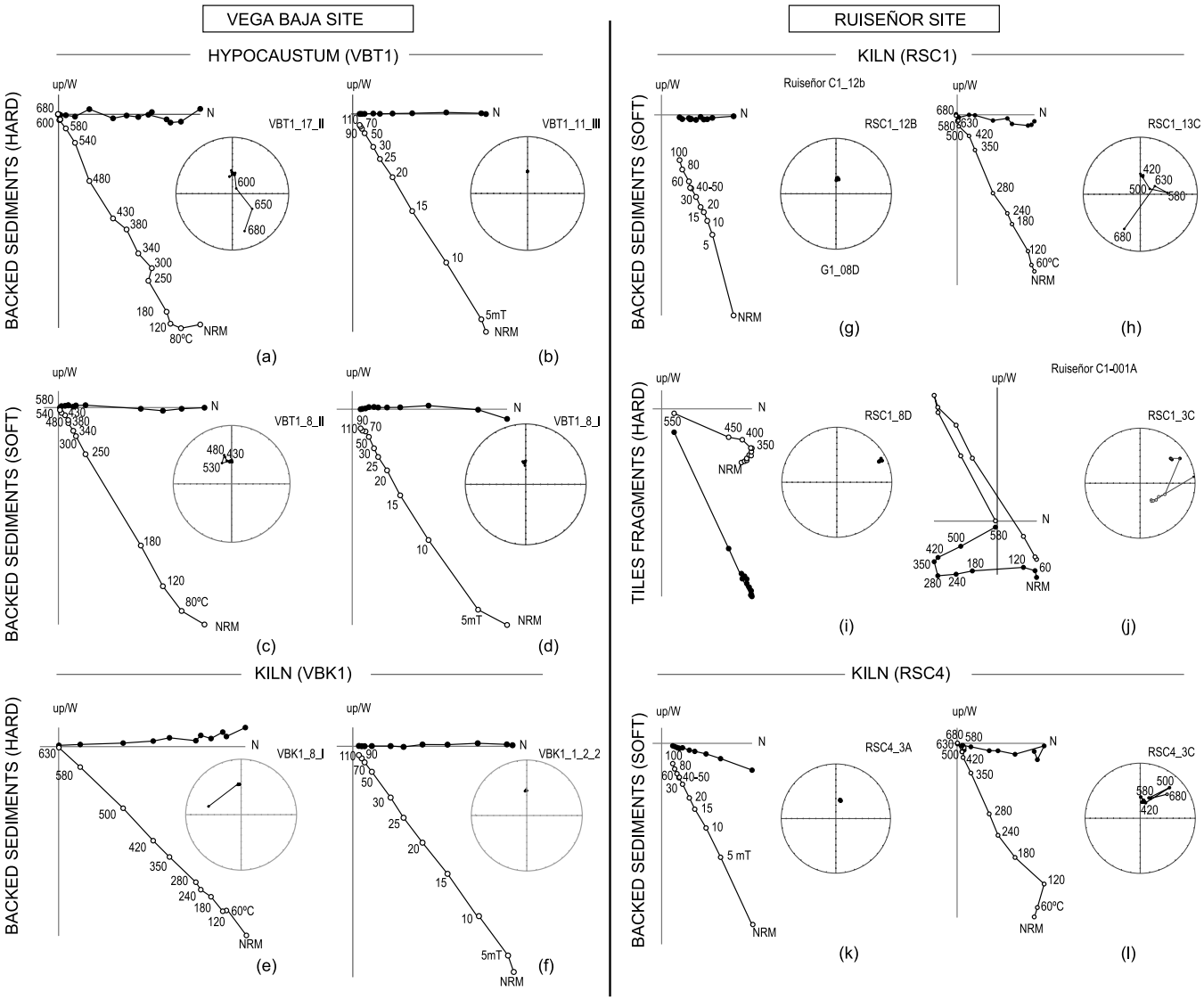

Figure 7. Representative orthogonal vector projections of the remanent magnetization (Zijderveld diagrams) obtained from stepwise thermal (TH) and alternating field (AF) demagnetization. Left-hand panel: Vega Baja, right-hand panel: Ruiseñor. In the demagnetization diagrams the open (closed) symbols are projections upon vertical (horizontal) planes.

and 100–110 mT that represented between 75 and 95 per cent of the initial NRM. The soft baked clays tended to exhibit higher proportions of AF-resistant NRM, with between 17 and 25 per cent of NRM remaining after 100 mT (e.g. Figs 8b and d). AF demagnetization was used with one tile specimen only, as it did not separate the magnetic components observed during thermal treatment.

For both the hard and soft baked clay specimens the stable components isolated by AF or TH yielded similar directions. This direction has been considered the characteristic remanent magnetization (ChRM) direction and is most likely related to a TRM acquired during the last use of the relevant structures. With respect to the tile specimens, great circle analysis (Fig. 9d) indicated a common northerly direction of the demagnetization trajectories that coincided with the best-fit directions obtained from the two linear, low temperature components and is in broad agreement with the directions obtained from the baked clay specimens from the same kiln. Therefore the low unblocking temperature component is considered the ChRM component, associated with the last use of the kiln. The high unblocking temperature component carries dispersed directions and is most probably associated with the TRM acquired during original fabrication of the tiles.

The mean direction for each structure has been calculated by combining the best-fit directions obtained from both AF and TH demagnetization of the soft and hard baked clays. Two specimens were rejected for RSC1 and RSC4 due to poorly defined demagnetization curves and incomplete isolation of the ChRM component. The directions obtained from the tile fragments have not been used due to the incomplete isolation of the ChRM component. A hierarchical approach was adopted (Lanos *et al*. 2005), taking the mean of specimens from the same (independently oriented) sample, followed by the mean between samples, using Fisher (1953) statistics. The results are shown in Fig. 9 and summarized in Table 3. They are characterized by low semi-angles of confidence α_{95} ($<3^{\circ}$) and high precision parameters, k, and thus represent well defined mean directions.

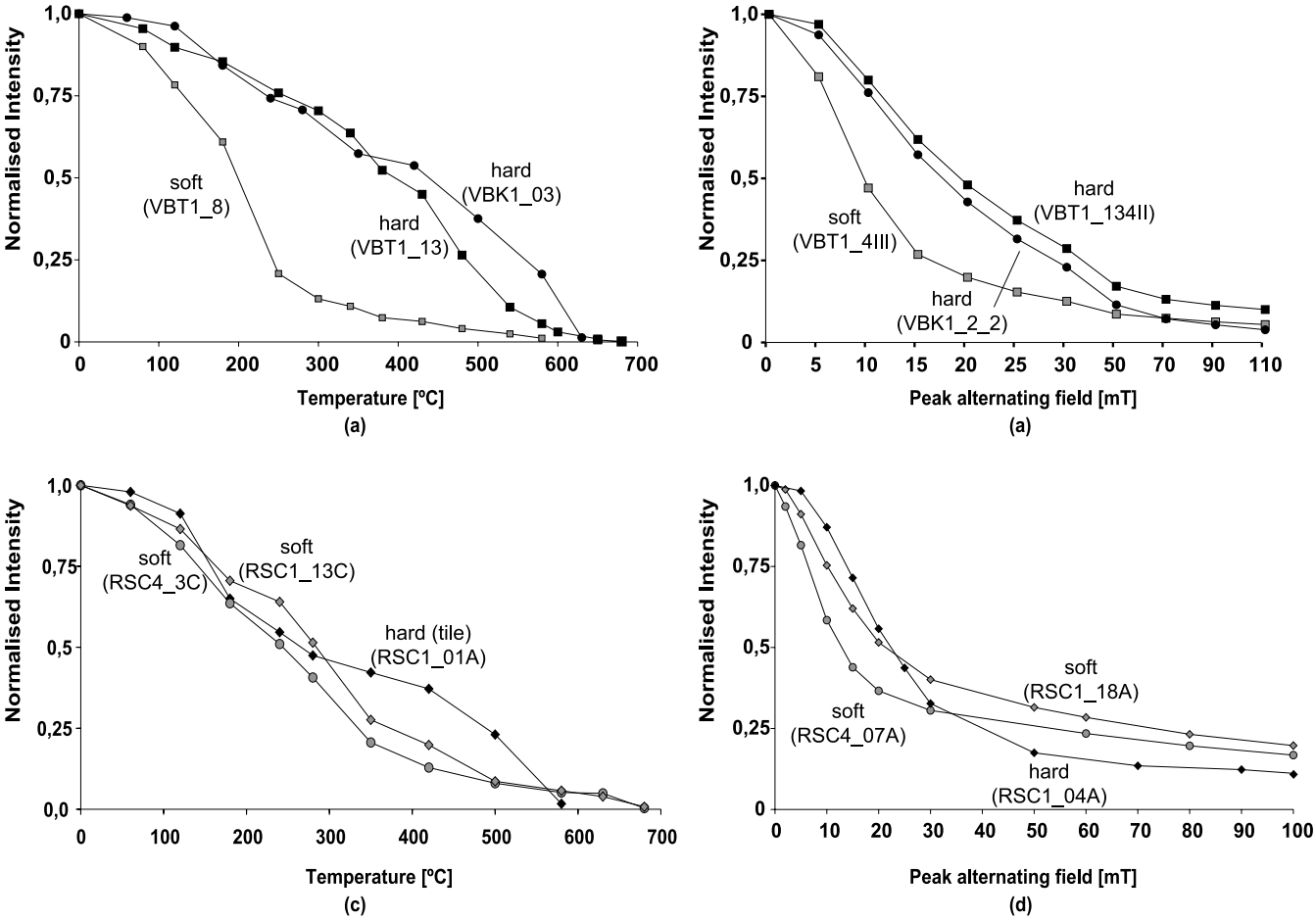

Figure 8. Representative natural remanent magnetization decay curves.

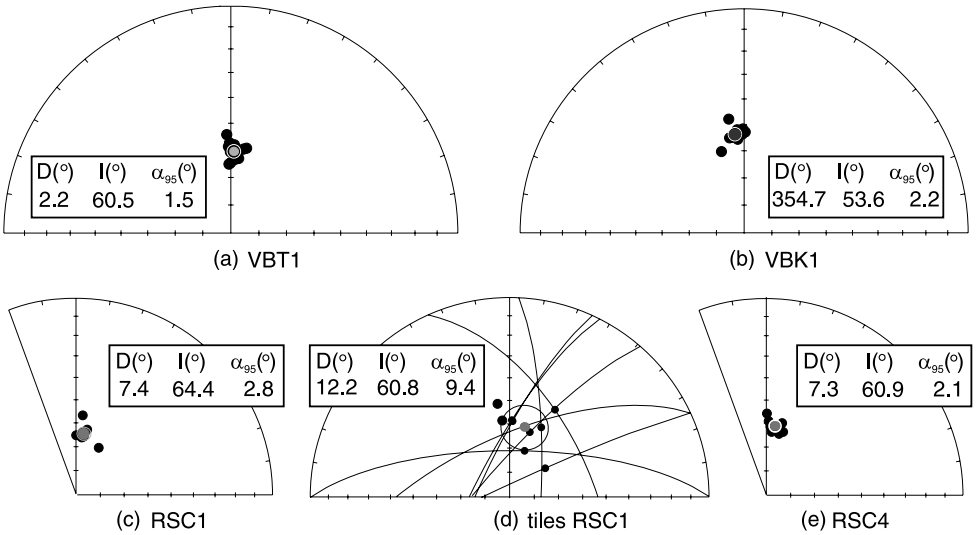

Figure 9. Stereoplots of characteristic remanent magnetization directions at the specimen level (black symbols), together with the mean direction and α_{95} (in grey) for each of the new structures studied. RSC1 tile samples have been treated separately from the rest of the RSC1 specimens (c). Remagnetization circles were used to determine mean RSC1 tile directions.

6 ARCHAEOINTENSITY DETERMINATIONS

Archaeointensity determinations were attempted on 23 specimens (from independent samples) from Ruiseñor and on 15 from Vega Baja. For the former, nine tile fragments from RSC1 and 14 soft baked sediments specimens from RSC1 and RSC4 structures were selected. From Vega Baja, two soft baked sediments specimens from VBT1 and six and seven hard baked sediment samples from VBT1 and VBK1 structures, respectively, were analysed.

Table 3. Site-mean characteristic remanent magnetization directions for the studied sites. N, Number of independently oriented samples used for the calculation; D, declination; I, inclination α_{95}, semi-angle of confidence; k, precision parameter and r_{sum}, resultant vector (Fisher 1953).

	N	D	I	α_{95}	k	r_{sum}	Age
RSC1	9	7.4°	64.5°	2.8°	339	8.976	450–700 AD
RSC4	10	7.3°	60.9°	2.1°	544	9.983	450–700 AD
VBT1	16	2.2°	60.5°	1.5°	571	15.974	596–657 AD
VBK1	11	354.7°	53.6°	2.2°	441	10.977	249–384 AD

Results were interpreted using NRM-TRM diagrams together with the corresponding Zijderveld plots. As expected, success of archaeointensity experiments depended on the type of material analysed. Only specimens corresponding to hard material and well-defined single components of magnetization trending toward the origin (VBK1 and VBT1) gave reliable results. Here, high quality linear NRM-TRM diagrams (with successful pTRM checks) were obtained (Figs 10a–d). This component is very stable and has been interpreted to be the TRM acquired during the last use of the structures. The last point retained for archaeointensity determination corresponds to the last temperature step before any evidence of changes in the magnetic mineralogy, detected by changes in pTRM acquisition or by the concave-up shapes on NRM-TRM plots (Hervé *et al*. 2011). Maximum temperature steps between 430 and 565 °C have been retained. The other group of specimens shows a more complex or unstable behaviour during Thellier experiments. This group corresponds to soft baked sediments specimens which were rejected due to the poor stability of the magnetic phase during heating, and the tile fragments that did not gave any useful results due to the difficulty in isolating the different remanent magnetization components (Figs 10e and f). In order to consider only high quality archaeointensity determinations these more complicated specimens have not been considered for further analysis. The archaeomagnetic behaviour observed during Thellier experiments results is in agreement with the rock magnetic and demagnetization experiments described in Sections 4 and 5.

Several criteria were used to select specimens with high quality archaeointensity determinations. Here the same acceptance criteria as those described by Gómez-Paccard *et al*. (2006c) have been used. Thirteen specimens gave reliable archaeointensity results (Table 4). All the results retained meet the acceptance criteria with the exception of one (specimen VBK1–6), for which the CRM parameter, i.e. the maximum potential error to the intensity caused by chemical remanent magnetization defined by Chauvin *et al*. (2005), is slightly higher than 15. As the other parameters meet the quality criteria this specimen has also been retained.

The influence of the anisotropy of the TRM and of the cooling time upon TRM intensity was investigated following the protocol described in Gómez-Paccard *et al*. (2006c). TRM anisotropy correction upon intensity estimates were calculated for all the specimens, except for three that broke during the experiments. Low TRM corrections were generally obtained, with differences between the uncorrected and corrected TRM values lower than 5 per cent. Only specimens VBK1–8 and VBT1–5 gave higher results: 6.4 and 16.0 per cent, respectively. To calculate mean site intensities, TRM anisotropy corrected values were retained when available (10 from the 13 studied specimens, see Table 4). The cooling rate effect was also investigated in all the specimens except two, which also broke during the experiments. Archaeological information suggests that the natural cooling time for the analysed structures could be much higher than typical laboratory cooling times (about 1.5 hr). Although no strong evidence of the real ancient cooling time is available, a cooling time of about 24 hr has been used to perform the cooling rate protocol. Comparison between rapid (about 1.5 hr) and slow cooling results (about 24 hr) has been used to quantify the cooling rate effect upon TRM intensity estimates at a specimen level (Table 4). Cooling rate correction factors were generally low (<5.5 per cent) except for specimens VBK1–9 and VBT1–20-I for which correction factors of 14.8 and 8.0 per cent were obtained, respectively.

In general, archaeointensity determinations from specimens from the same structure were very similar (e.g. VBK1–1 and -8 or VBT1–15-II and –16-I). However, some differences were also observed (e.g., VBK1–4 or VBT1–20-I). This highlights the need to study several independent samples per structure to obtain accurate mean intensities. Weighted mean-site intensities were calculated using the weighting factor per specimen proposed by Prévot *et al*. (1985). This procedure takes into account the different qualities of the archaeointensity determinations at specimen level as expressed by the quality parameters given in Table 4 (Coe *et al*. 1978; Prévot *et al*. 1985).

Two mean intensities of 64.2 ± 5.0 and 62.4 ± 2.6 μT were obtained for VBK1 and VBT1, respectively. They have been derived from Thellier classical experiments including TRM anisotropy and cooling rate corrections performed on several independent samples per site. The standard deviations around the means are lower than 10 per cent in both cases. As both the cooling rate and the TRM anisotropy effects upon TRM intensity are low, very similar standard deviations are found before and after the corrections. Therefore the mean site intensities obtained can be considered as highly reliable.

7 DISCUSSION AND CONCLUSIONS

7.1 Degree of heating and the suitability of baked clays for archaeomagnetism

The material studied here consisted of baked clays with varying degrees of hardness, with the hardness governed by the heating temperatures. The hard baked clay (and tile) samples have suffered the highest temperatures and their magnetic properties are dominated by magnetite or thermally stable maghaemite. These minerals are often present in the original clay material. Heating may also give rise to the formation of new ferrimagnetic phases, for example through the reduction of haematite (Evans & Heller 2003) or the alteration of iron oxyhydroxides (Gendler *et al*. 2005). Such magnetic enhancement is a common feature of baked clays and probably explains the high values of the concentration-dependent parameters observed in this study. If the formation of these new phases preceded the last heating and cooling of the baked clays, then such material is ideal for archaeomagnetic studies—as the wealth of studies over the last 100 yr or more has shown.

The soft baked clays appear to have suffered a much lower degree of heating and they are much less magnetic than the hard baked clays. Magnetic enhancement is much less pronounced and they probably preserve more of their original iron oxide mineralogy, including a detectable haematite contribution. Whilst this does not necessarily mean that they are incapable of acquiring a stable TRM, poorly or moderately heated clay material presents two main problems for archaeomagnetism. The first is that their low degree of physical stability makes field sampling and laboratory sub-sampling

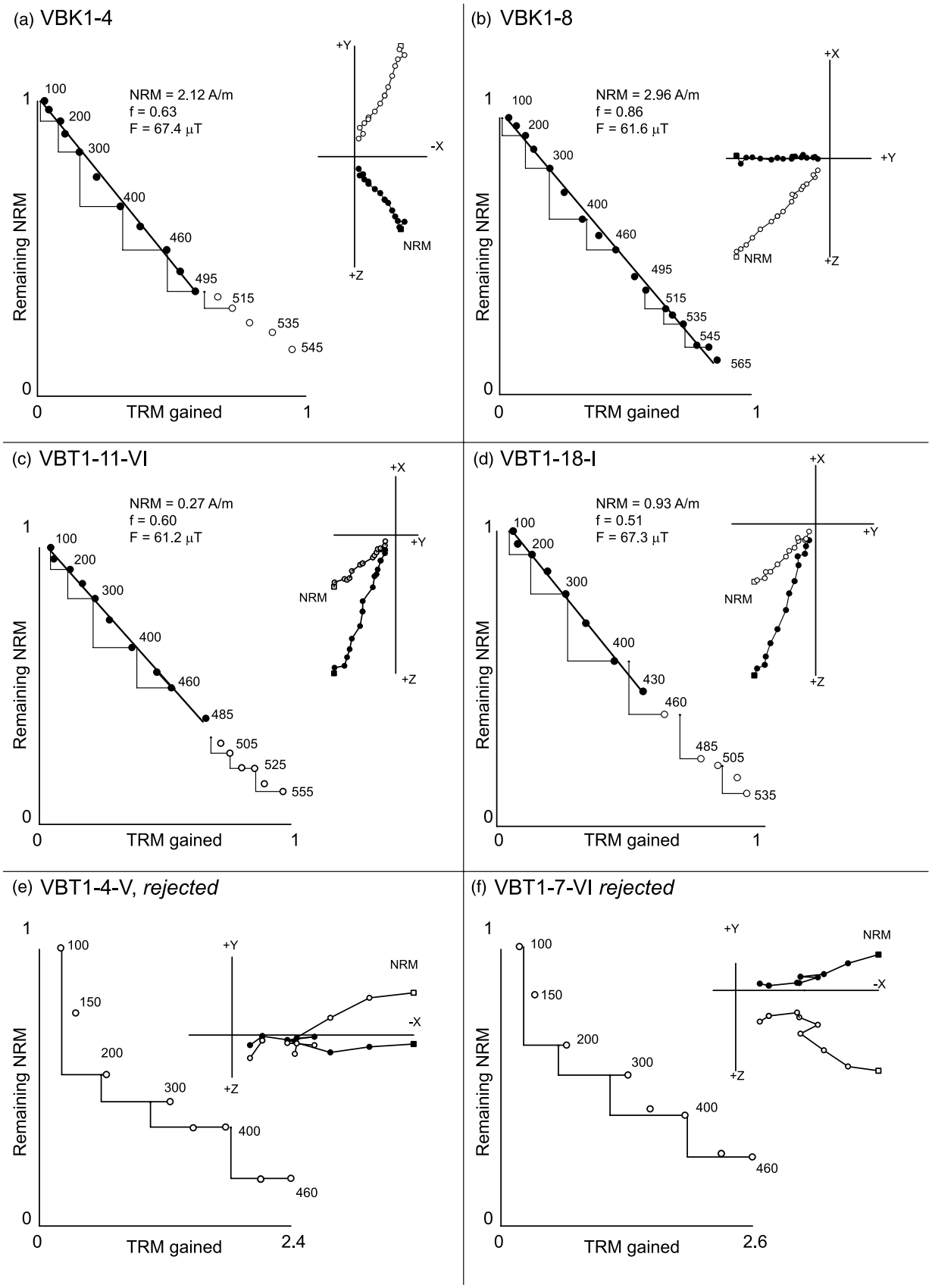

Figure 10. Examples of typical NRM-TRM diagrams for Vega Baja specimens together with orthogonal vector projections of the remanent magnetization in sample coordinates. Open (solid) circles are projections upon vertical (horizontal) planes. Diagrams are normalized to the initial NRM intensity. Closed circles in the NRM-TRM diagrams are data used for the archaeointensity determinations. The field obtained (F) together with the percentage of the initial NRM involved in the slope calculation (f parameter) are indicated.

Table 4. Summary of archaeointensity results. Name, name of the structure studied; Spe., specimen number; NRM, intensity of the natural remanent magnetization; χ, initial susceptibility (SI units); $T_{min} - T_{max}$, temperature interval used for the slope calculation; *n*, number of data points within this temperature interval; *f*, fraction of the NRM component used in the slope calculation; *g*, gap factor; *q*, quality factor; MAD, maximum angle of deviation; DANG, deviation angle; CRM, potential error on the estimation of the palaeointensity due to the acquisition of CRM as a percentage of the applied field (Chauvin *et al*. 2005); $F \pm$ S.D., intensity and standard deviation per specimen without TRM anisotropy correction; Fe, intensity per specimen corrected for TRM anisotropy; $Fm \pm S.D.$, TRM anisotropy corrected mean intensity per site and standard deviation; *Fpo*, weighted mean intensity per site; ΔM (24 hr), correction factor per specimen for a cooling time of about 24 hr; *Fpocr*, weighted mean intensity per site after TRM anisotropy and cooling rate corrections; *Fma*, mean intensity per site relocated to Madrid; VDM and VADM, values of the virtual dipole moment and virtual axial dipole moment.

Name	Spe.	NRM (A m^{-1})	χ (10^{-6})	$T_{min} - T_{max}$ (°C)	*n*	*f*	*g*	*q*	MAD (°)	DANG (°)	CRM (per cent)	$F \pm$ S.D. (μT)	F_e (μT)	$Fm \pm$ S.D. (μT)	*Fpo* (μT)	ΔM (24 hr) (per cent)	Alt. (24 hr) (per cent)	*Fpocr* (μT)	*Fma* (μT)	VDM (10^{22} Am^2)	VADM (10^{22} Am^2)
VBK1	1	2.47	7390	100–565	19	0.87	0.92	47.8	4.8	2.2	5.2	62.1 ± 1.0	64.1	67.2 ± 3.5	66.6	5.1	0.4	64.2 ± 5.0	64.6	11.9	11.1
	3	1.82	5190	100–460	8	0.60	0.85	21.8	3.3	5.4	6.6	64.2 ± 1.5									
	4	2.12	4520	100–495	12	0.63	0.89	26.1	4.7	2.1	8.4	67.4 ± 1.4	71.0			4.8	1.9				
	5	2.48	5530	100–460	9	0.55	0.86	25.8	4.5	2.9	6.4	64.9 ± 1.2									
	6	3.33	6760	100–460	10	0.53	0.86	16.6	4.6	2.4	15.5	71.3 ± 2.0	73.0			4.2	4.4				
	8	2.96	6100	100–565	19	0.86	0.93	45.8	3.6	1.2	4.7	61.6 ± 1.1	65.8			3.9	1.9				
	9	2.70	5740	100–460	10	0.49	0.86	15.3	4.5	0.8	12.5	66.4 ± 1.8	67.1			14.8	3.3				
VBT1	115-VI	0.27	2890	100–485	11	0.60	0.87	23.5	5.9	1.9	4.7	61.2 ± 1.4	62.7	65.4 ± 3.4	65.2	5.3	0.9	62.4 ± 2.6	62.7	10.6	10.8
	13-V	2.31	6180	100–460	10	0.55	0.86	16.0	4.5	3.0	5.2	70.5 ± 2.1	60.5			2.0	0.5				
	15-II	1.94	5080	100–485	11	0.57	0.88	16.9	5.1	2.7	7	66.3 ± 2.0	65.5			2.2	0.3				
	16-I	2.54	5650	100–485	11	0.58	0.87	14.9	5.1	2.0	9.7	66.9 ± 2.2	66.1			2.0	1.9				
	18-I	0.93	3230	100–430	8	0.51	0.84	18.5	4.0	2.0	3.3	67.3 ± 1.6				5.2	4.0				
	20-I	1.21	3880	100–460	10	0.56	0.86	14.4	2.8	0.9	4.1	71.1 ± 2.4	70.2			8.0	5.9				

difficult. As shown in this study, careful sampling procedures, along with consolidation where necessary, can overcome this difficulty.

Second, and more importantly, soft baked clays tend to undergo thermally induced alteration during laboratory heating (e.g., Jordanova *et al*. 2003). As such they are often avoided in archaeomagnetic studies. The thermal instability clearly affects the results of Thellier-type intensity experiments. None of the soft baked clay specimens studied here yielded a reliable archaeointensity determination. However, they did provide a well-defined archaeomagnetic direction that was isolated by AF demagnetization (to 100 mT) or by thermal demagnetization up to 400–430 °C. For the RSC1 and RSC4 structures, whose mean directions were defined from soft baked clay specimens only, the mean directions displayed α_{95} values less than 3° (Table 3). This is more than adequate for both geomagnetic and archaeomagnetic dating purposes.

It is worth highlighting these results as they demonstrate that poorly consolidated baked clays that may have only been heated to moderate temperatures may still be suitable for directional studies. The baked clays in this study have an NRM that is predominantly carried by ferrimagnetic minerals and both AF and TH demagnetization could be used to isolate their characteristic directions. In clays with a similar proportion of low coercivity magnetic minerals, similarly positive results might be expected.

7.2 New archaeomagnetic data for Western Europe and geomagnetic models

The four new archaeomagnetic directions obtained in this study have been compared with the archaeomagnetic Spanish database (Gómez-Paccard *et al*. 2006a) and with the dataset used to derive the PSV curve for Iberian Peninsula (Gómez-Paccard *et al*. 2006b), which also includes data from northern Morocco and southern France relocated to Madrid coordinates via the virtual geomagnetic pole (Figs 11a and b).

Directions from the oldest structure, VBK1, are consistent with the previous Iberian archaeomagnetic directional dataset. The three data from RSC1, RSC4 and VBT1 cover the lack of Iberian archaeomagnetic information for the early Middle Age period. They are in agreement with the archaeomagnetic data from southern France.

The new data help in defining the beginning of the easterly shift in declination of the geomagnetic field that was initiated around 350–400 AD and culminated around 800–850 AD. In addition the new data confirm the maximum in inclination suggested by Bayesian Iberian SV curve, which took place around 600–650 AD.

The recently developed regional geomagnetic model (SCHA.DIF.3K) of Pavón-Carrasco *et al*. (2009) predicts variations, both in declination and inclination, that are confirmed by the new data of this study (Figs 11c and d). In addition, the new data are also in agreement with the latest global geomagnetic model (ARCH3K.1, Korte *et al*. 2009).

Fig. 12(a) shows the new archaeointensity data from this study together with the available data from southwestern Europe (including northern Morocco) relocated to Madrid. The SW Europe database is still scarce, but consistent. It delineates a coherent trend of palaeointensity variations from 200 BC up to 600 AD and from 1050 AD up to 1600 AD. A relative maximum is observed at around 1550 AD, followed by a probably sharp minimum. A considerable gap is still observed between 600 AD and 1050 AD and few data are available after 1600 AD.

In order to compare the new intensities with other previous data from Western Europe, they have been relocated to the latitude of

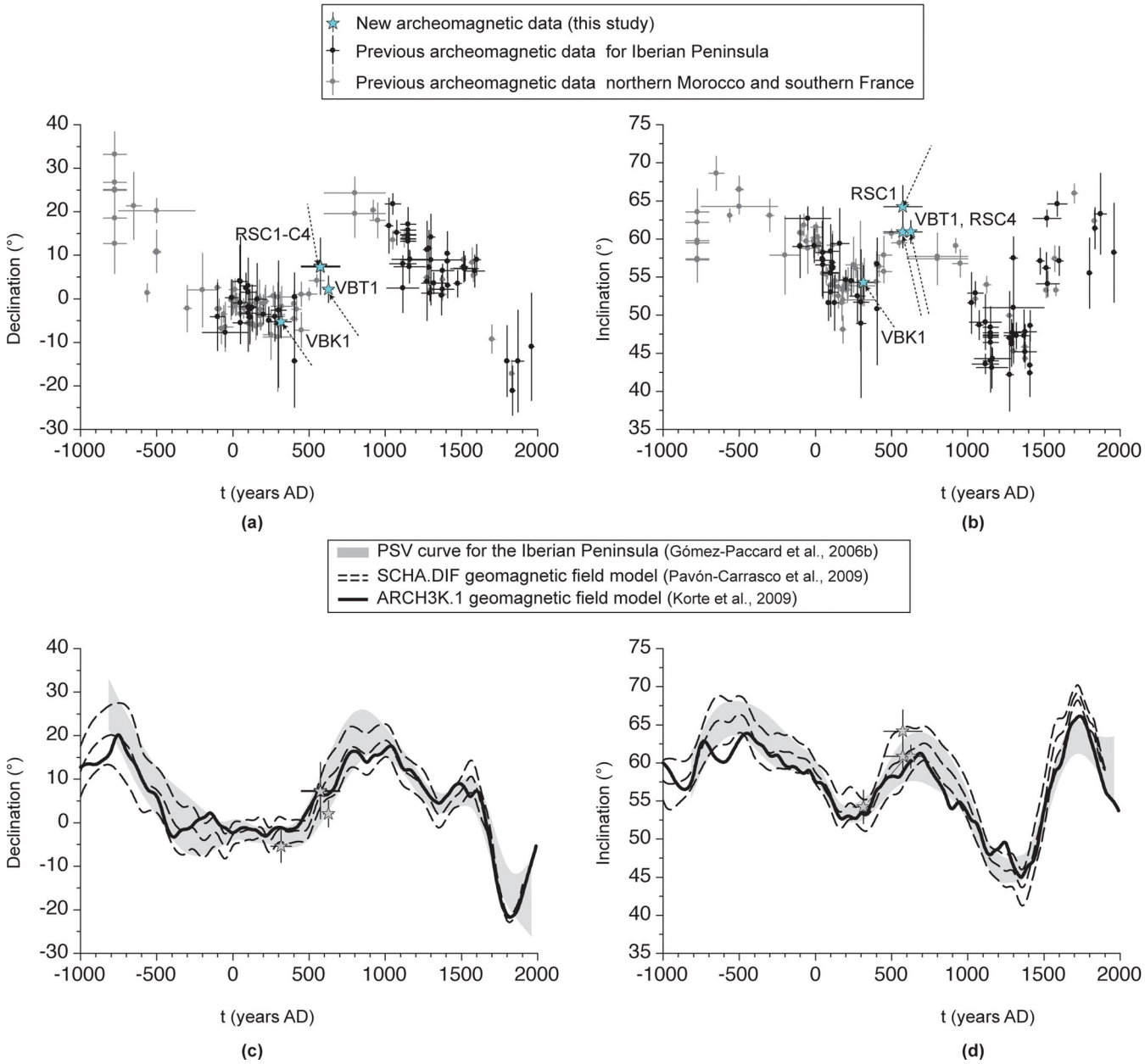

Figure 11. Declination (a) and inclination (b) values of archaeomagnetic data reduced to the reference site of Madrid. The new data are plotted (stars, highlighted by the dashed arrows) together with previous available data from the Iberian Peninsula (black dots) and northern Morocco and southern France (grey dots). In (c) and (d) the PSV curve for the Iberian Peninsula obtained from Bayesian modelling (Gómez-Paccard *et al*. 2006b) and the regional SCHA.DIF.3K and ARCH3K.1 global geomagnetic field model results (Pavón-Carrasco *et al*. 2009, Korte *et al*. 2009) are also shown. The grey area in the Iberian PSV curve corresponds to the 95 per cent error envelope.

Paris through the virtual axial dipole moment (VADM). Previous data available from Spain, Portugal, France, northern Morocco, Belgium and Switzerland have also been compiled. For this purpose the archaeointensity compilation of Genevey *et al*. (2008) has been supplemented with new data from Gómez-Paccard *et al*. (2008), Donadini *et al.* (2008), Spassov *et al*. (2008), Genevey *et al*. (2009), Gallet *et al*. (2009) and Hartmann *et al*. (2009). Fig. 12(b) shows the new archaeointensity data obtained for central Spain together with the mentioned compiled data from Western Europe.

The intensity obtained for the VBK1 site is in good agreement with previous results and indicates an intensity value of around 70 μT during the 4th century in Western Europe. No data are available in this region for the time of the VBT1 structure. This new data constrains the starting age of the strong maximum in intensity that occurred around 850 AD (Genevey & Gallet 2002; Donadini *et al*. 2008; Gallet *et al*. 2009).

The new intensity results have also been compared with the intensity reference curve available for Western Europe (Gómez-Paccard *et al*. 2008) and with the results derived from the regional (Pavón-Carrasco *et al*. 2009) and global (Korte *et al*. 2009) geomagnetic field models (Fig. 12b). A reference intensity curve for Western Europe (Gómez-Paccard *et al*. 2008) was derived using

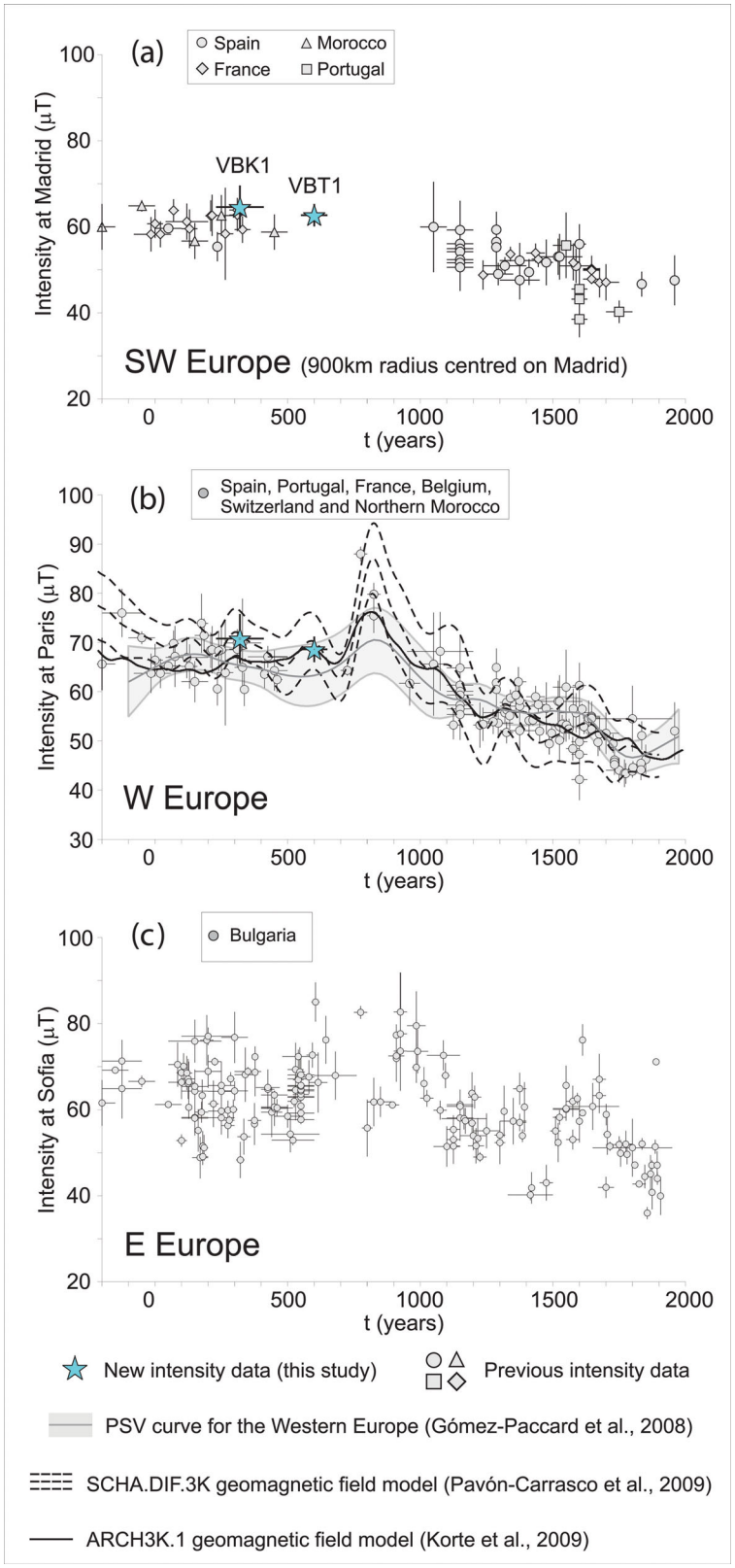

Figure 12. (a) Comparison between the new archaeointensity data obtained in this study (black stars) and previous available data for the Iberian Peninsula, northern Morocco, southern France and Portugal (Gómez-Paccard *et al*. 2008; Hartmann *et al*. 2009; Kovacheva *et al*. 2009). All data and curves are relocated to the latitude of Madrid. (b) Comparison between the new archaeointensity data and previous archaeointensity data available for Western Europe (see Genevey *et al*. 2009 and references therein). The reference curve available for Western Europe (Gómez-Paccard *et al*. 2008), the results derived from the regional SCHA.DIF.3K and ARCH3K.1 global geomagnetic field model (Pavón-Carrasco *et al*. 2009, Korte *et al*. 2009) are also shown. The grey area in the Western European curve corresponds to the 95 per cent error envelope. All data and curves are relocated to the latitude of Paris. (c) The archaeointensity database from Bulgaria (Kovacheva *et al*. 2009). All data relocated to Sophia coordinates.

Bayesian statistics (Lanos 2004) and a selection of the most reliable data available in 2008 from Western Europe. The Bayesian reference curve for Western Europe is clearly too smooth to describe the detailed evolution of geomagnetic field intensity changes. The global ARCH3K.1 archaeomagnetic model, based on archaeomagnetic data derived from archaeological material and volcanic rocks recently published by Korte *et al*. (2009), and the regional SCHA.DIF.3K archaeomagnetic model—only based on archaeomagnetic data, derived from archaeological structures—available for Europe (Pavón-Carrasco *et al*. 2009), have also been used for comparison. The new archaeointensity data from this study are in a reasonably good agreement with both models and the entire Western Europe database fit very well the mean curve derived from the SCHA.DIF.3K model. Both data and model results suggest that two relatively minor intensity maxima took place in Western Europe around 320 and 600 AD before the high maximum that took place around 850 AD.

It is worthwhile noting that no previous archaeomagnetic data were available for the Iberian Peninsula between 500 and 1000 AD, and only five data were published from Western Europe for this time period. Very few data are still available for the Middle Ages in Western Europe, in a period when both global and regional models predict that the geomagnetic field reached its highest intensity of the last 2000 yr.

The Western Europe database has also been compared with the recent compiled database from Eastern Europe (the Bulgarian database, Kovacheva *et al*. 2009), shown in Fig. 12(c). It provides more data for the considered time period. There, a maximum that occurred between 600 and 650 AD is clearly recorded. This maximum is suggested by the new data from this study, but its magnitude is lower, or it occurred after the age of the VBT1 structure. In addition, variations more rapid than those predicted by the models could also have occurred during the 600–1000 AD time interval, according to the Eastern Europe database. Pavón-Carrasco *et al*. (2009) proposed the existence of a rapid change of geomagnetic field around 775–825 AD and suspected another rapid change around 650–700 AD. However, more data are still necessary to confirm the latter.

Finally, the rate of intensity field variations that occurred during the early Middle Ages seems to be higher than previously expected by global geomagnetic field models. According to the SCHA.DIF.3K regional model (Pavón-Carrasco *et al*. 2009), and corroborated by recent results, the rate of increase in palaeointensity, observed at Paris, between 700 and 800 AD is about $0.22 \pm 0.11\ \mu\mathrm{T\ yr^{-1}}$, followed by a decrease (between 800 and 1000 AD) of about $-0.12 \pm 0.10\ \mu\mathrm{T\ yr^{-1}}$. These are higher values than the rate of decay estimated for the period 1650 and 1900 AD (around $-0.02 \pm 0.04\ \mu\mathrm{T\ yr^{-1}}$) from both the regional SCHA.DIF.3K and the global GUFM1 (Jackson *et al.* 2000) models. They are also even higher than the rate of decrease observed in the last century in southern Africa, of about $-0.1\ \mu\mathrm{T\ yr^{-1}}$, according to the 11th IGRF model. In terms of dipolar decay, from 900 to 1900 AD, the estimated rate is $14 \pm 2\ \mathrm{nT\ yr^{-1}}$ according to SCHA.DIF.3K (or $5.0 \pm 0.5\ \mathrm{nT\ yr^{-1}}$ predicted by the ARCH3K.1) and for the 800–1000 AD it is about $48 \pm 1\ \mathrm{nT\ yr^{-1}}$, higher than the decay of the last century, $18\ \mathrm{nT\ yr^{-1}}$ (11th IGRF, Finlay *et al*. 2010). Are these rapid intensity variations real or are they an artefact produced by palaeointensity determinations? The extreme variation of the geomagnetic field that seems to be occurred during the Middle Age period (the highest produced in historical times) should be studied more in depth to help in the understanding of present day field variations.

ACKNOWLEDGMENTS

We would like to express our considerable thanks to I. Ramírez and A.J. Gómez-Laguna in allowing us to take all the necessary samples from the archaeological structures. Their considerable interest and support on this project made possible this research. The authors would like to express their sincere thanks to Dr. Christian Dietz for helping during sampling at Ruiseñor site and to Elisabet Beamud for helping with archaeointensity measurements. We are very grateful for the thoughtful reviews of Dr. Fabio Donadini and a second, anonymous referee, who both helped improve the final manuscript. This work has been carried out within the National Plan for Scientific Investigation, Development, and Technological Innovation (I+D+i) 2008–2011 and cofinanced by the Spanish Ministry of Science and Innovation in the frame of the 'Programma de Técnicos de Apoyo (2008/2011)'. It has been funded by the Spanish Ministry of Science and Technology (grants SAB2008–0181 and CGL2008–02203/BTE and CGL2011–24790), the European Union (HPRN-CT-2002–00219), and the Complutense University, Comunidad de Madrid Consolidación de grupos program (910396). Financial support to this research was also given by a CSIC JAE-Doc postdoctoral research contract (MGP).

REFERENCES

Bronk Ramsey, C., 2009. Bayesian analysis of radiocarbon dates, *Radiocarbon,* **51**(1), 337–360.

Bucur, I., 1994. The direction of the terrestrial magnetic field in France during the last 21 centuries: recent progress, *Phys. Earth planet. Inter.,* **87**(1–2), 95–109, doi:10.1016/0031-9201(94)90024-8.

Catanzariti, G., McIntosh, G., Osete, M.L., Nakamura, T., Rakowski, A.Z., Ramiréz-González, I. & Lanos, P., 2007. A comparison of radiocarbon and archaeomagnetic dating from an archaeological site in Spain. *Radiocarbon,* **49,** 543–550.

Catanzariti, G., McIntosh, G., Gómez-Paccard, M., Ruiz-Martínez, V.C., Osete, M.L., Chauvin, A. & the AARCH scientific team, 2008. Quality control of archaeomagnetic determination using a modern kiln with a complex NRM, *Phys. Chem. Earth,* **33**(6–7), 427–437.

Chauvin, A., Roperch, P. & Levi, S., 2005. Reliability of geomagnetic paleointensity data: the effects of the NRM fraction and concave up behaviour on paleointensity determination by Thellier method, *Phys. Earth planet. Inter.,* **150,** 265–286.

Coe, R.S., Grommé, S. & Mankinen, E.A., 1978. Geomagnetic paleointensities from radiocarbon-dated lava flows on Hawaii and the question of the Pacific non dipole low, *J. geophys. Res.,* **83**(B4), 1740–1756.

Donadini, F., Kovacheva M., Kostadinova, M., Hedley, I.G. & Pesonen, L.J., 2008. Palaeointensity determination on an early medieval kiln from Switzerland and the effect of cooling rate, *Phys. Chem. Earth,* **33**(6–7), 449–457.

Donadini, F., Korte, M. & Constable, C.G., 2009. Geomagnetic field for 0–3 ka: 1. New data sets for global modeling, *Geochem. Geophys. Geosyst.,* **10**(6), Q06007, doi:10.1029/2008GC002295.

Evans, M.E. & Heller, F., 2003. *Environmental Magnetism: Principles and Applications of Environmagnetics,* Academic Press, San Diego, CA.

Finlay, C.C. *et al*., 2010. International geomagnetic reference field: the eleventh generation, *Geophys. J. Int.,* **183,** 1216–1230, doi:10.1111/j.1365-246X.2010.04804.x

Fisher, R.A., 1953. Dispersion on a sphere, *Proc. R. Soc. Lond. Ser. A,* **217,** 295, doi:10.1098/rspa.1953.0064.

Gallet, Y., Genevey, A. & Le Goff, M., 2002. Three millennia of directional variation of the Earth's magnetic field in western Europe as revealed by archaeological artefacts, *Phys. Earth planet. Inter.,* **131**(1), 81–89, doi:10.1016/S0031-9201(02)00030-4.

Gallet, Y., Genevey, A., Le Goff, M., Warmé, N., Gran-Aymerich, J. & Lefevre, A., 2009. On the use of archeology in geomagnetism, and vice-versa: recent developments in archeomagnetism, *C. R. Physique,* **10**(7), 630–648.

Gendler, T.S., Shcherbakov, V.P., Dekkers, M.J., Gapeev, A.K, Gribov, S.K. & McClelland, E., 2005. The lepidocrocite-maghemite-haematite reaction chain—I. Acquisition of chemical remanent magnetization by maghemite, its magnetic properties and thermal stability, *Geophys. J. Int.,* **160,** 815–832.

Genevey, A. & Gallet, Y., 2002. Intensity of the geomagnetic field in western Europe over the past 2000 years: new data from ancient French potteries, *J. geophys. Res.,* **107,** doi:10.1029/2001JB000701.

Genevey, A., Gallet, Y., Constable, C.G., Korte, M. & Hulot, G., 2008. ArcheoInt: an upgraded compilation of geomagnetic field intensity data for the past ten millennia and its application to the recovery of the past dipole moment, *Geochem. Geophys. Geosyst.,* **9**(4), Q04038, doi:10.1029/2007GC001881.

Genevey, A., Gallet, Y., Rosen, J. & Le Goff, M., 2009. Evidence for rapid geomagnetic field intensity variations in Western Europe over the past 800 years from new French archeointensity data, *Earth planet. Sci. Lett.,* **284**(1–2), 132–143. doi:101.1016/j.epsl.2009.04.024.

Gómez-Paccard, M. *et al*., 2006a. A catalogue of Spanish archaeomagnetic data, *Geophys. J. Int.,* **166,** 1125–1143, doi:10.1111/j.1365-246X.2006.03020.x.

Gómez-Paccard, M., Chauvin, A., Lanos, P., McIntosh, G., Osete, M.L., Catanzariti, G., Ruiz-Martínez, V.C. & Núñez, J.I., 2006b. First archaeomagnetic secular variation curve for the Iberian Peninsula: comparison with other data from western Europe and with global geomagnetic field models, *Geochem. Geophys. Geosyst.,* **7,** Q12001, doi:10.1029/2006GC001476.

Gómez-Paccard, M., Chauvin, A., Lanos, P., Thiriot, J. & Jiménez-Castillo, P., 2006c. Archeomagnetic study of seven contemporaneous kilns from Murcia (Spain), *Phys. Earth planet. Inter.,* **157**(1–2), 16–32, doi:10.1016/j.pepi.2006.03.001.

Gómez-Paccard, M., Chauvin, A., Lanos, P. & Thiriot, J., 2008. New archeointensity data from Spain and the geomagnetic dipole moment in western Europe over the past 2000 years, *J. geophys. Res.,* **113**(B9), B09103.

Hartmann, G.A., Trindade, R.I.F., Goguitchaichvili, A., Etchevarne, C., Morales, J. & Afonso, M.C., 2009. First archeointensity results from Portuguese potteries (1550–1750 AD), *Earth Planets Space,* **61**(1), 93–100.

Hervé, G., Schnepp, E., Chauvin, A., Lanos, P. & Nowaczyk, N., 2011. Archaeomagnetic results on three Early Iron Age salt-kilns from Moyenvic (France), *Geophys. J. Int.,* **185,** 144–156, doi:10.1111/j.1365-246X.2011.04933.x

Iasonov, P.G., Nurgaliev, D.K., Burov, D.V. & Heller, F., 1998. A modernized coercivity spectrometer, *Geologica Carpathica,* **49**(3), 224–226.

Jordanova, N., Kovacheva, M., Hedley, I. & Kostadinova, M., 2003. On the suitability of baked clay for archaeomagnetic studies as deduced from detailed rock-magnetic studies, *Geophys. J. Int.,* **153,** 146–158.

Jackson, A., Jonkers, R.T. & Walker, M.R., 2000. Four centuries of geomagnetic secular variation from historical records, *Phil. Trans. R. Soc. Lond. A,* **358,** 957–990.

Kovacheva, M., Jordanova, N. & Karloukovski, V., 1998. Geomagnetic field variations as determined from Bulgarian archaeomagnetic data. Part II: the last 8000 years, *Surv. Geophys.,* **19**(5), 431–460, doi:10.1023/A:1006502313519.

Kovacheva, M., Boyadziev, Y., Kostadinova-Avramova, M., Jordanova, N. & Donadini, F., 2009. Updated archeomagnetic data set of the past 8 millennia from the Sofia laboratory, Bulgaria, *Geochem. Geophys. Geosyst.,* **10,** Q05002.

Korte, M., Donadini, F. & Constable, C.G., 2009. Geomagnetic field for 0–3 ka: 2. A new series of time-varying global models, *Geochem. Geophys. Geosyst.,* **10,** Q06008, doi:10.1029/2008GC002297.

Lanos, P., 2004. Bayesian inference of calibration curves: application to archaeomagnetism, in *Tools for Constructing Chronologies: Crossing Disciplinary Boundaries,* Lecture Notes in Statistics, Vol. 177, pp. 43–82, eds Buck, C.E. & Millard, A.R., Springer, London.

Lanos, P., Le Goff, M., Kovacheva M. & Schnepp, E. 2005. Hierarchical modelling of archaeomagnetic data and curve estimation by moving average technique. *Geophys. J. Int.,* **160,** 440–476.

Pavón-Carrasco, F.J., Osete, M.L., Torta, J.M. & Gaya-Pique, L.R., 2009. A regional archaeomagnetic model for Europe for the last 3000 years, SCHA.DIF.3K: applications to archaeomagnetic dating, *Geochem. Geophys. Geosyst.,* **10,** doi:10.1029/2008GC002244.

Pavón-Carrasco, F.J., Rodríguez-González, J., Osete, M.L. & Torta, M., 2011. A Matlab tool for archaeomagnetic dating, *J. Archaeol. Sci.,* **38,** 408–419.

Prévot, M., Mankinen, E.A., Coe, R.S. & Grommé, C.S., 1985. The Steens Mountain (Oregon) geomagnetic polarity transition. 2. Field intensity variations and discussion of reversal models, *J. geophys. Res.*, **90,** 10 417–10 448.

Ramírez-González, I., 2008. Informe de la Excavación Arqueológica de El Ruiseñor (Guadalajara), in *Informe de la Junta de Comunidades de Castilla la Mancha,* pp. 56–59, Guadalajara.

Reimer, P. J. *et al*., 2009. IntCal09 and Marine09 radiocarbon age calibration curves, 0–50,000 years cal BP, *Radiocarbon,* **51**(4), 1111–1150.

Ruiz-Martinez, V.C., Pavón-Carrasco, F.J. & Catanzariti, G., 2008. First archaeomagnetic data from northern Iberia, *Phys. Chem. Earth,* **33**(6–7), 566–577.

Rojas, J.M. & Gómez-Laguna, A.J., 2009. Intervención arqueológica en la Vega Baja de Toledo. Características del centro político y religioso del reino visigodo, in *El siglo VII frente al siglo VII: Arquitectura. Anejos de AEspALI,* pp. 45–90, eds Caballero-Zoreda, L., Mateos-Cruz, P. & Utrero-Agudo, M.A., Consejo Superior de Investigación Cientifica (CSIC), Madrid.

Spassov, S., Hus, J., Geeraerst, R. & Heller, F., 2008. Archaeomagnetic dating of a High Middle Age likely iron working site in Corroy-le-Grand (Belgium), *Phys. Chem. Earth,* **33**(6–7), 544–556.

Tauxe, L., 1998. *Paleomagnetic Principles and Practice*. Kluwer, Amsterdam, 299 pp.

Thellier, E. & Thellier, O., 1959. Sur l'intensité du champ magnétique terrestre dans le passé historique et géologique, *Ann. Géophys.,* **15,** 285–376.

Vigil-Escalera A., 2007. Poblamiento rural de época visigoda en el sector norte del territorio toledano, in *AA.VV., Hispania Gothorum. San Ildefonso y el Reino Visigodo de Toledo,* pp. 107–114, Junta Comunidades Castilla La Mancha, Toledo.